CHEMISTRY
A EUROPEAN JOURNAL

FULL PAPER

DOI: 10.1002/chem.201302378

High-Pressure Synthesis and Characterization of New Actinide Borates, AnB_4O_8 (An = Th, U)

Ernst Hinteregger,[a] Thomas S. Hofer,[a] Gunter Heymann,[a] Lukas Perfler,[b] Florian Kraus,[c] and Hubert Huppertz*[a]

Abstract: New actinide borates ThB_4O_8 and UB_4O_8 were synthesized under high-pressure, high-temperature conditions (5.5 GPa/1100 °C for thorium borate, 10.5 GPa/1100 °C for the isotypic uranium borate) in a Walker-type multianvil apparatus from their corresponding actinide oxide and boron oxide. The crystal structure was determined on basis of single-crystal X-ray diffraction data that were collected at room temperature. Both compounds crystallized in the monoclinic space group $C2/c$ ($Z=4$). Lattice parameters for ThB_4O_8: $a=1611.3(3)$, $b=419.86(8)$, $c=730.6(2)$ pm; $\beta=114.70(3)°$; $V=449.0(2)$ Å^3; $R_1=0.0255$, $wR_2=0.0653$ (all data). Lattice parameters for UB_4O_8: $a=1589.7(3)$, $b=422.14(8)$, $c=723.4(2)$ pm; $\beta=114.13(3)°$; $V=443.1(2)$ Å^3; $R_1=0.0227$, $wR_2=0.0372$ (all data). The new AnB_4O_8 (An = Th, U) structure type is constructed from corner-sharing BO_4 tetrahedra, which form layers in the bc plane. One of the four independent oxygen atoms is threefold-coordinated. The actinide cations are located between the boron–oxygen layers. In addition to Raman spectroscopic investigations, DFT calculations were performed to support the assignment of the vibrational bands.

Keywords: actinides · borates · density functional theory · high-pressure chemistry · Raman spectroscopy

Introduction

Over the last decade, our research into the high-pressure chemistry of borates has led to the synthesis of several new compounds with fascinating structures, owing to the efficient use of the multianvil technique.[1] For example, we discovered the rare-earth borate $Dy_4B_6O_{15}$,[2] which was the first borate that exhibited edge-sharing BO_4 tetrahedra. Later on, HP-NiB_2O_4 was synthesized,[3] which was the first borate in which all of the $[BO_4]^{5-}$ tetrahedra showed a linkage through a common edge to a second tetrahedron, as well as HP-KB_3O_5,[4] which simultaneously contained all three possible conjunction modes, that is, corner-sharing BO_3 groups, corner-sharing BO_4 units, and edge-sharing BO_4 tetrahedra.

Following our interest in the high-pressure chemistry of alkali, alkaline-earth, transition-metal, and rare-earth borates, we decided to broaden our research activities into the field of actinide borates. This field of structural chemistry is highly topical, as reflected by the considerable number of new actinide borates with interesting structures and properties that have been synthesized within the last few years.[5–11] A closer look at the existing compounds with An-B-O ternary systems only showed a few phases. Just six compounds with the actinide cations thorium, uranium, and americium are known, namely: $Th(B_2O_5)$,[12] $ThB_{66.8}O_{0.36}$,[13] $U(BO_3)_2$,[14] $(UO_2)(B_2O_4)$,[12] AmB_9O_{18},[11] and $AmBO_3$.[15] To the best of our knowledge, no ternary actinide borates have been synthesized under high-pressure conditions so far. However, recent studies on the chemistry of high-pressure alkaline uranyl borates demonstrated the feasibility of this approach.[10] Historically, Berzelius has already reported the possible presence of a thorium borate in a mineral that was found in Norway in 1824.[16] Furthermore, there are several existing hydrated actinide borates of the actinides thorium, uranium, neptunium, plutonium, and americium. Research into actinide borates is of urgent importance in the question of the storage of nuclear waste. Owing to the high stability and insolubility of borates, they are of interest for the immobilization of nuclear waste. In this context, borates in which the metal cation is in the oxidation state 4+ have a special position, because the cation (especially cerium) can be regarded as a "dummy" for plutonium, owing to their comparable ionic radii. Herein, we describe the syntheses, single-

[a] E. Hinteregger, Dr. T. S. Hofer, Dr. G. Heymann, Prof. Dr. H. Huppertz
Institute of General, Inorganic and Theoretical Chemistry
Leopold-Franzens-Universität Innsbruck
Innrain 80–82, 6020 Innsbruck (Austria)
Fax: (+43) 512-507-57099
E-mail: hubert.huppertz@uibk.ac.at

[b] L. Perfler
Institute of Mineralogy and Petrography
Leopold-Franzens-Universität Innsbruck
Innrain 52 f, 6020 Innsbruck (Austria)

[c] Priv.-Doz. Dr. F. Kraus
AG Fluorchemie, Department Chemie
Technische Universität München
Lichtenbergstrasse 4, 85747 Garching (Germany)

crystal structural determinations, and Raman spectroscopic investigations of AnB_4O_8 (An = Th, U), as well as quantum-chemical calculations of the harmonic vibrational frequencies of ThB_4O_8.

Results and Discussion

Synthesis and crystal-structure analysis: The compounds ThB_4O_8 and UB_4O_8 were synthesized from their corresponding actinide oxides and B_2O_3 under high-pressure, high-temperature conditions (5.5 GPa and 1100 °C for ThB_4O_8; 10.5 GPa and 1100 °C for UB_4O_8) in a 1000 ton multianvil press that was fitted with a Walker-type module. A detailed description of the syntheses is provided in the Experimental Section. Figure 1 shows the diffraction patterns of ThB_4O_8 (top) and UB_4O_8 (bottom), as well as reflections of the corresponding actinide oxide (marked with lines) and reflections of another still-unknown side product (marked with circles). The single-crystal intensity data were collected at room temperature on a Nonius Kappa-CCD diffractometer with graphite-monochromated $Mo_{K\alpha}$ radiation (λ = 71.073 pm). Tables 1, Table 2, and Table 3 list the details of the data collection and evaluation, as well as the positional parameters of the refinement. Interatomic distances and interatomic angles are listed in Table 4 and Table 5.

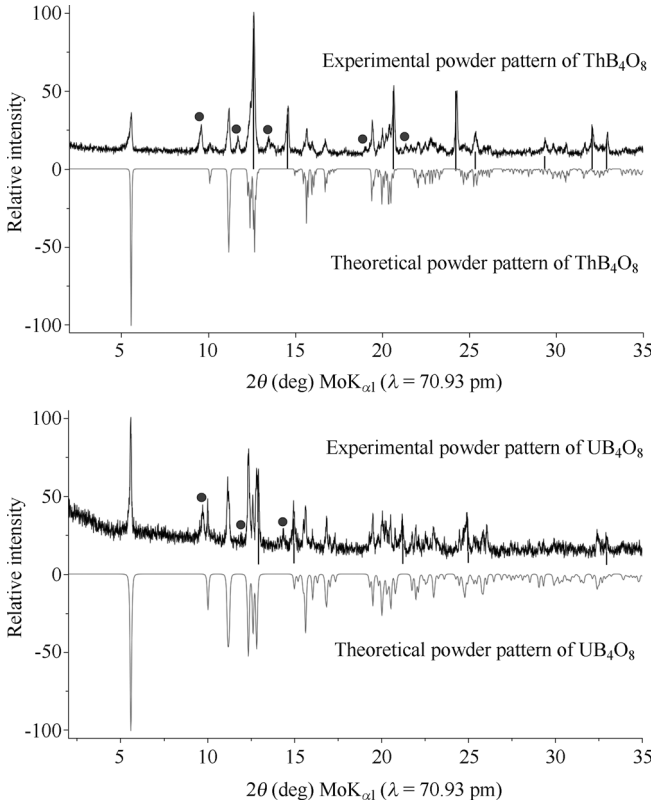

Figure 1. Top: Experimental and theoretical powder X-ray diffraction (PXRD) patterns of ThB_4O_8 (space group $C2/c$); the reflections of an unknown phase are indicated by circles. The reflections of ThO_2 are marked with lines. Bottom: Experimental and theoretical PXRD patterns of UB_4O_8 (space group $C2/c$); reflections of an unknown phase are indicated by circles. The reflexions of $UO_{2.12}$ are marked with lines. The theoretical PXRD patterns are based on the single-crystal diffraction data.

Table 1. Crystal data and structure refinement of AnB_4O_8 (An = Th, U; space group $C2/c$); standard deviations are given in parentheses.

Empirical formula	ThB_4O_8	UB_4O_8
molar mass [g mol^{-1}]	403.28	409.27
crystal system	monoclinic	monoclinic
space group	$C2/c$ (No. 15)	$C2/c$ (No. 15)
Single-crystal data		
single-crystal diffractometer	Enraf–Nonius Kappa CCD	Enraf–Nonius Kappa CCD
radiation	$Mo_{K\alpha}$ (λ = 71.073 pm)	$Mo_{K\alpha}$ (λ = 71.073 pm)
a [pm]	1611.3(3)	1589.7(3)
b [pm]	419.86(8)	422.14(8)
c [pm]	730.6(2)	723.4(2)
β [°]	114.70(3)	114.13(3)
V [Å^3]	449.0(2)	443.1(2)
formula units per cell	4	4
ρ_{calcd} [g cm^{-3}]	5.97	6.14
crystal size [mm^3]	0.08 × 0.15 × 0.05	0.02 × 0.02 × 0.01
T [K]	293(2)	293(2)
μ [mm^{-1}]	33.22	36.64
F(000)	696	704
θ range [°]	2.8–30.0	2.8–30.0
range in hkl	±22, ±5, ±10	±22, ±5, ±10
total no. of reflections	2400	2382
independent reflections	655 (R_{int} = 0.0495)	640 (R_{int} = 0.0561)
reflections with [$I \geq 2\sigma(I)$]	653 (R_σ = 0.0345)	602 (R_σ = 0.0387)
data/parameters	655/61	640/61
absorption correction	multi-scan (Scalepack[46])	multi-scan (Scalepack[46])
GOF on F_i^2	1.175	1.059
final R indices [$I \geq 2\sigma(I)$]	R_1 = 0.0254	R_1 = 0.0187
	wR_2 = 0.0652	wR_2 = 0.0365
R indices (all data)	R_1 = 0.0255	R_1 = 0.0227
	wR_2 = 0.0653	wR_2 = 0.0372
largest diff. peak/hole [e Å^{-3}]	5.925/−1.990	1.512/−1.191

Table 2. Atomic coordinates, Wyckoff positions, and equivalent isotropic displacement parameters (U_{eq} [Å^2]) of AnB_4O_8 (An = Th, U; space group $C2/c$); standard deviations are given in parentheses.[a]

Atom	Wyckoff position	x	y	z	U_{eq}
Th1	4e	0	0.19317(4)	0.25	0.0035(2)
O1	8f	0.2163(3)	0.146(2)	0.1675(7)	0.0033(7)
O2	8f	0.3428(3)	0.152(2)	0.4908(7)	0.0042(8)
O3	8f	0.3678(4)	0.3026(7)	0.2043(8)	0.0044(9)
O4	8f	0.4480(3)	0.261 (2)	0.0129(7)	0.0057(8)
B1	8f	0.3038(5)	0.304(2)	0.296(2)	0.003(2)
B2	8f	0.3584(6)	0.189(2)	0.008(2)	0.004(2)
U1	4e	0	0.16767(6)	0.25	0.0048(2)
O1	8f	0.2163(2)	0.1454(8)	0.1679(5)	0.0041(6)
O2	8f	0.3452(2)	0.1510(9)	0.4929(5)	0.0050(6)
O3	8f	0.3688(2)	0.3048(8)	0.2012(5)	0.0033(6)
O4	8f	0.4484(2)	0.2652(8)	0.0038(6)	0.0066(7)
B1	8f	0.3049(4)	0.304(2)	0.2961(8)	0.004(2)
B2	8f	0.3603(4)	0.187(2)	0.0062(8)	0.006(2)

[a] U_{eq} is defined as one third of the trace of the orthogonalized U_{ij} tensor.

Table 3. Anisotropic displacement parameters (U_{ij} [Å^2]) for AnB$_4$O$_8$ (An = Th, U; space group: $C2/c$); standard deviations are given in parentheses.

Atom	U_{11}	U_{22}	U_{33}	U_{12}	U_{13}	U_{23}
Th1	0.0032(2)	0.0050(2)	0.0028(2)	0	0.0018(2)	0
O1	0.002(2)	0.003(2)	0.004(2)	0.000(2)	0.000(2)	0.001(2)
O2	0.007(2)	0.003(2)	0.003(2)	−0.001(2)	0.002(2)	0.001(2)
O3	0.002(2)	0.008(2)	0.005(2)	−0.001(2)	0.003(2)	0.000(2)
O4	0.008(2)	0.006(2)	0.005(2)	0.000(2)	0.004(2)	0.000(2)
B1	0.002(3)	0.005(3)	0.001(3)	−0.001(2)	−0.001(3)	0.001(2)
B2	0.004(3)	0.004(3)	0.003(3)	0.001(2)	0.002(3)	0.000(2)
U1	0.0044(2)	0.0053(2)	0.0047(2)	0	0.0021(2)	0
O1	0.003(2)	0.006(2)	0.002(2)	0.000(2)	−0.001(2)	0.000 (2)
O2	0.007(2)	0.002(2)	0.006(2)	0.001(2)	0.002(2)	0.001(2)
O3	0.004(2)	0.004(2)	0.003(2)	0.000(2)	0.002(2)	−0.001(2)
O4	0.005(2)	0.006(2)	0.012(2)	−0.002(2)	0.006(2)	−0.002(2)
B1	0.003(2)	0.006(2)	0.003(2)	−0.001(2)	0.000(2)	−0.001(2)
B2	0.009(3)	0.005(2)	0.005(2)	−0.002(2)	0.005(2)	0.002(2)

Table 4. Interatomic distances [pm] in AnB$_4$O$_8$ (An = Th, U; space group $C2/c$), as calculated from the single-crystal lattice parameters; standard deviations are given in parentheses.

	ThB$_4$O$_8$		UB$_4$O$_8$
Th1−O4	240.3(5) (×2)	U1−O4	231.4(4) (×2)
Th1−O4′	240.4(5) (×2)	U1−O4′	235.3(4) (×2)
Th1−O2	253.3(5) (×2)	U1−O3	249.4(5) (×2)
Th1−O3	259.7(5) (×2)	U1−O2	252.2(4) (×2)
Th1−O4″	285.9(5) (×2)	U1−O4″	300.2(4) (×2)
	Ø = 255.9		Ø = 253.7
B1−O2	144.3(8)	B1−O3	144.0(6)
B1−O3	144.3(9)	B1−O2	145.1(6)
B1−O1	148.4(8)	B1−O1	149.1(8)
B1−O1′	152.1(6)	B1−O1′	152.8(6)
	Ø = 147.3		Ø = 147.8
B2−O2	145.0(5)	B2−O2	144.5(6)
B2−O3	146.0(9)	B2−O4	144.6(7)
B2−O4	146.0(9)	B2−O3	144.8(6)
B−O1	150.9(8)	B2−O1	152.1(7)
	Ø = 147.0		Ø = 146.5

Table 5. Interatomic angles [°] in AnB$_4$O$_8$ (An = Th, U; space group $C2/c$), as calculated from the single-crystal lattice parameters; standard deviations are given in parentheses.

ThB$_4$O$_8$			
O3-B1-O2	110.8(6)	O2-B2-O4	109.9(5)
O3-B1-O1	112.3(5)	O2-B2-O3	110.4(5)
O2-B1-O1	109.5(4)	O4-B2-O3	102.2(5)
O3-B1-O1′	109.3(4)	O2-B2-O1	109.5(5)
O2-B1-O1′	106.3(5)	O4-B2-O1	110.9(5)
O1-B1-O1′	108.5(5)	O3-B2-O1	113.7(5)
	Ø = 109.5		Ø = 109.4
UB$_4$O$_8$			
O3-B1-O2	110.7(4)	O2-B2-O4	111.0(4)
O3-B1-O1	112.1(4)	O2-B2-O3	110.5(4)
O2-B1-O1	109.7(4)	O4-B2-O3	103.2(4)
O3-B1-O1′	109.0(4)	O2-B2-O1	110.4(4)
O2-B1-O1′	107.0(4)	O4-B2-O1	109.6(4)
O1-B1-O1′	108.1(4)	O3-B2-O1	111.9(4)
	Ø = 109.4		Ø = 109.4

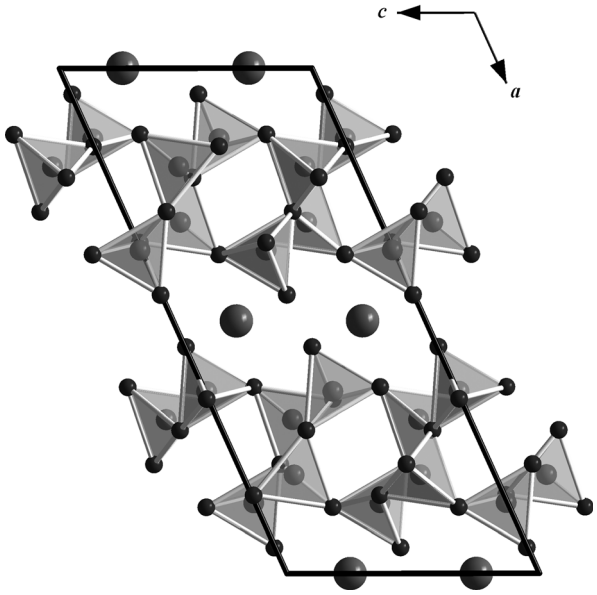

Figure 2. Crystal structure of the new actinide borates AnB$_4$O$_8$ (An = Th, U; space group $C2/c$) along the b axis, which shows layers of linked [BO$_4^{5-}$] groups.

Crystal structures: The new isotypic actinide borates ThB$_4$O$_8$ and UB$_4$O$_8$ crystallize in the monoclinic space group $C2/c$, with four formula units per unit cell. Lattice parameters for ThB$_4$O$_8$: a = 1611.3(3), b = 419.86(8), c = 730.6(2) pm; β = 114.70(3)°; V = 449.0(2) Å^3. Lattice parameters for UB$_4$O$_8$: a = 1589.7(3), b = 422.14(8), c = 723.4(2) pm; β = 114.13(3)°; V = 443.1(2) Å^3. Figure 2 shows the crystal structure of AnB$_4$O$_8$ (An = Th, U) along the b axis, which is comprised of layers of corner-sharing [BO$_4$]$^{5-}$ tetrahedra that are separated by layers of actinide cations. As in most high-pressure borates, such as RE_4B$_6$O$_{15}$ (RE = Dy, Ho[2,17]), α-RE_2B$_4$O$_9$ (RE = Sm–Tb, Ho[18–21]), and the rare-earth meta-borates δ-RE(BO$_2$)$_3$ (RE = Ce, La[22,23]), this structure is exclusively built up from tetrahedral borate groups. Figure 3 shows the composition of the borate layers. A closer look at the layers exhibits infinite chains along the b axis, which consist of [B2O$_4$]$^{5-}$ tetrahedra that are connected through one common oxygen atom, O3 (Figure 3, large spheres). These chains of [B2O$_4$]$^{5-}$ tetrahedra and antiparallel-orientated chains alternate along the c axis and are linked together through the common oxygen atoms of the [B1O$_4$]$^{5-}$ and [B2O$_4$]$^{5-}$ tetrahedra (O1, O2, and O3). Figure 4 shows the layers along the a, b, and c directions. The BO$_4$ groups form a central "dreier ring", a "vierer ring", and different "sechser rings".[24] The corners of the "dreier rings" are formed from two O3 atoms and one O2 atom that are located along the b axis. The "vierer rings" are composed of two [B1O$_4$]$^{5-}$ groups and two [B2O$_4$]$^{5-}$ groups that are linked together through the O2 and O3 atoms; these "vierer rings" form empty channels along the b axis, as shown in Figure 4. These rings can be represented by a unit that is comprised of five [B2O$_4$]$^{5-}$ groups and four

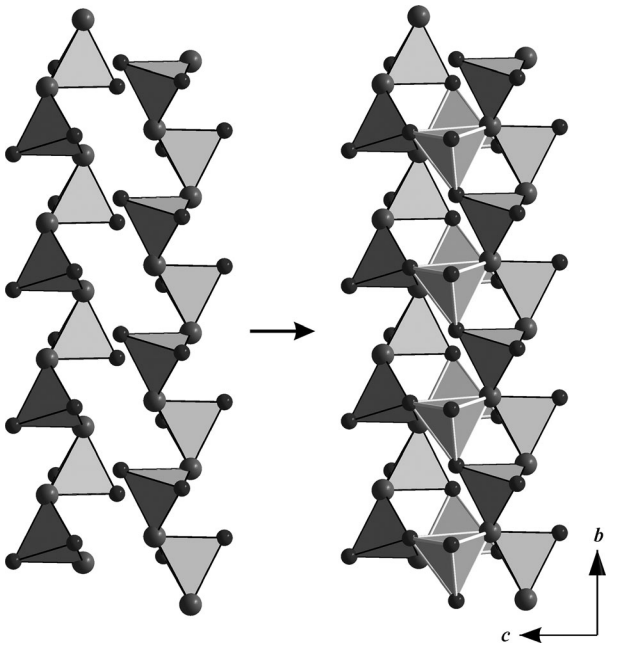

Figure 3. Crystal structure of AnB_4O_8 (An=Th, U; space group $C2/c$). Left: Chains of corner-sharing $[B2O_4]^{5-}$ tetrahedra along the b axis, which are linked by the threefold coordinated O3 atoms (large spheres). Right: $[B1O_4]^{5-}$ tetrahedra (light-colored edges) link together two borate chains through oxygen atoms O2, O3, and O4.

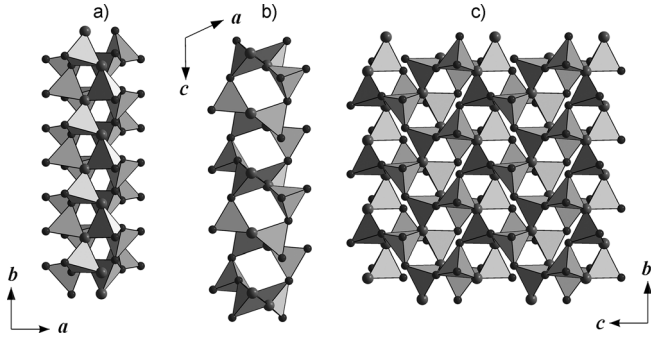

Figure 4. Crystal structure of AnB_4O_8 (An=Th, U; space group $C2/c$), which shows the borate layers in the bc plane.

$[B1O_4]^{5-}$ groups, as shown in Figure 5. The crystal structure of AnB_4O_8 (An=Th, U) contains four crystallographically distinguishable oxygen atoms: Oxygen atoms O1 and O2 are twofold-coordinated by boron atoms. Oxygen atom O4 is a terminal oxygen atom that is orientated towards the cation layer; a view along the c axis shows the terminal O4 oxygen atoms of the borate layers. The O3 oxygen atom is exceptional, in that it is a threefold-coordinated oxygen atom. Figure 6 shows the $[O3^{[3]}(BO_3)_3]^{11-}$ unit, which is comprised of two $[B2O_4]^{5-}$ tetrahedra and one $[B1O_4]^{5-}$ tetrahedron. The B-O3$^{[3]}$-B angles sum up to 360°, as expected from the trigonal-planar geometry. The two crystallographically distinguishable boron atoms in the actinide borates ThB_4O_8 and UB_4O_8 are tetrahedrally coordinated by four oxygen atoms. The mean values of the boron–oxygen distances inside the tetrahedra vary between 144.3(8) (B1–O2) and 152.1(6) pm (B2–O1), with a mean value of 147.2 pm for ThB_4O_8, and between 144.0(6) (B1–O3) and 152.1(7) pm (B2–O1), with a mean value of 147.2 pm for UB_4O_8. These values agree well with the known average value for the B–O distance in $[BO_4]^{5-}$ groups (147.6 pm).[25–27] The oxygen-boron-oxygen angles in the tetrahedral $[BO_4]^{5-}$ groups in AnB_4O_8 (An=Th, U) are listed in Table 5 and correspond well with the expected angles of tetrahedrally coordinated groups. Figure 7 shows the coordination sphere of the actinide cations in AnB_4O_8 (An=Th, U). Ten oxygen atoms coordinate to both the thorium and uranium cations. Owing to the two longest actinide–oxygen distances (Th1–O4″ = 285.9(5) pm (×2), U1–O4″ = 300.2(4) pm (×2)) and the large difference between the third-longest An–O distances (Th1–O3 = 259.7(5) pm, U1–O3 = 252.2(4) pm), the description as an 8+2 coordination mode for the Th1 and U1 atoms is reasonable. These coordination spheres result in thorium–oxygen distances of between 240.3(5) and

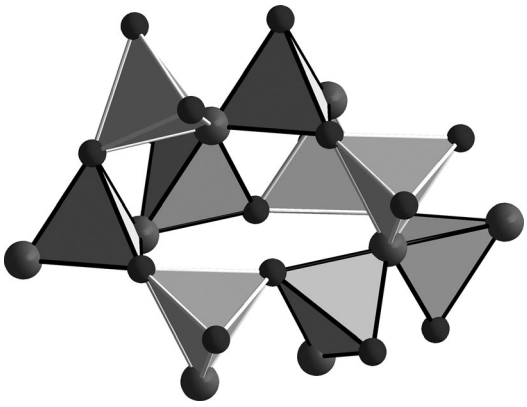

Figure 5. Unit of nine BO_4 groups, which contains a central "dreier ring", a "vierer ring", and different "sechser rings". $[B1O_4]^{5-}$ tetrahedra are denoted by light-colored edges and $[B2O_4]^{5-}$ tetrahedra are denoted by black edges. The threefold-coordinated oxygen atoms O3$^{[3]}$ are denoted as large spheres.

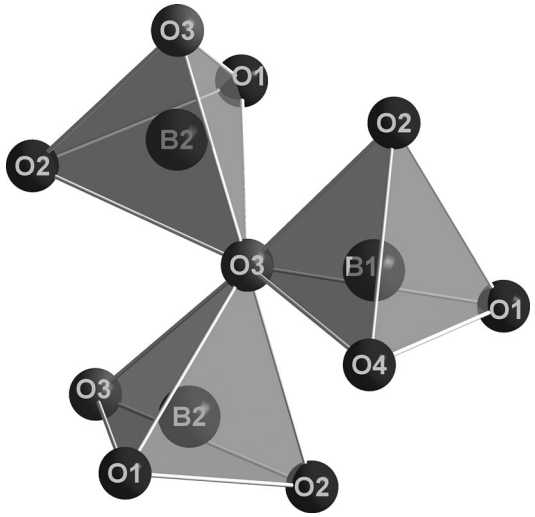

Figure 6. Threefold-coordinated oxygen atom (central sphere) in the crystal structure of AnB_4O_8 (An=Th, U; space group $C2/c$).

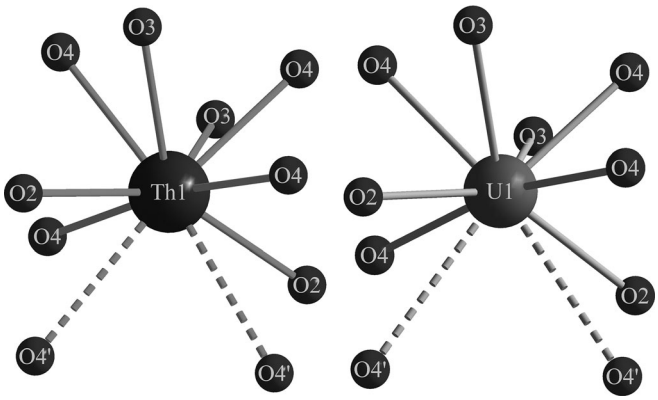

Figure 7. Coordination spheres of the actinide ions in AnB_4O_8 (An = Th, U; space group $C2/c$); both cations are surrounded by ten oxygen anions, which possess 8+2-fold coordination.

285.9(5) pm, with a mean value of 255.9 pm for Th1 in ThB_4O_8, and between 231.4(4) and 300.2(4) pm, with a mean value of 253.7 pm for the uranium cations in UB_4O_8. A closer look at the lattice parameters (a, b, and c; β) reveals a decrease in the a (−1.3%), c (−1.0%), and β parameters (−0.5%), in contrast to a slight increase in the b parameter (+0.5%) in the structures of UB_4O_8 and ThB_4O_8. This divergence emerges from the higher ionic radius of Th^{4+}. As expected, the An–O (An = U, Th) distances in ThB_4O_8 are larger, because of the larger ionic radius of Th^{4+}. A comparison of the tetrahedral borate groups shows no greater deviances in the bond lengths and angles. In addition, the bond-valence sums for all atoms of ThB_4O_8 and UB_4O_8 were calculated by using the bond-length/bond-strength (ΣV)[28,29] and CHARDI concepts (charge distribution in solids, ΣQ).[30] The results of these calculations are listed in Table 6. All of the calculated values correspond well with the expected values of the formal ionic charges.

Table 6. Charge distribution in AnB_4O_8 (An = Th, U; space group $C2/c$), as calculated by using the bond-length/bond-strength (ΣV)[28,29] and Chardi concepts (ΣQ).[30]

	Th1	B1	B2	O1	O2	O3	O4
ΣV	+3.79	+3.05	+3.07	−2.09	−2.00	−1.92	−2.00
ΣQ	+3.95	+3.03	+3.00	−1.94	−2.06	−1.96	−2.04
	U1	B1	B2	O1	O2	O3	O4
ΣV	+3.75	+3.01	+3.11	−2.05	−1.95	−1.99	−1.92
ΣQ	+3.92	+3.05	+2.99	−1.89	−2.01	−2.06	−2.04

Owing to the fact that the structure type of AnB_4O_8 (An=Th, U) is exclusively built up from BO_4 tetrahedra, one could imagine a structural relationship with the structures of well-known uranium and thorium silicates. However, both of the ThB_4O_8 and UB_4O_8 structures exhibit three-fold-coordinated oxygen atoms, a structural motif that is unknown in the chemistry of silicates. Therefore, there is no visible direct structural relationship.

MAPLE values (madelung part of lattice energy)[31–33] were calculated for comparison with the MAPLE values as obtained from the summation of the binary actinide oxides, ThO_2,[34] and UO_2,[35] and with that of the high-pressure modification B_2O_3-II.[36] Values of 55317 and 55569 kJ mol^{-1} were obtained for ThB_4O_8 and UB_4O_8, respectively, in comparison with 55421 kJ mol^{-1} (deviation = 0.2%) and 55721 kJ mol^{-1} deviation = 0.3%) for the corresponding binary oxides (ThO_2 (11544 kJ mol^{-1})+2 B_2O_3-II (2× 21938 kJ mol^{-1}); UO_2 (11544 kJ mol^{-1})+2× B_2O_3-II (2× 21938 kJ mol^{-1})).

Vibrational spectroscopy: Figure 8 shows the Raman spectra of single crystals of the actinide borates ThB_4O_8 and UB_4O_8 within the range 100–1500 cm^{-1}. No OH or water bands

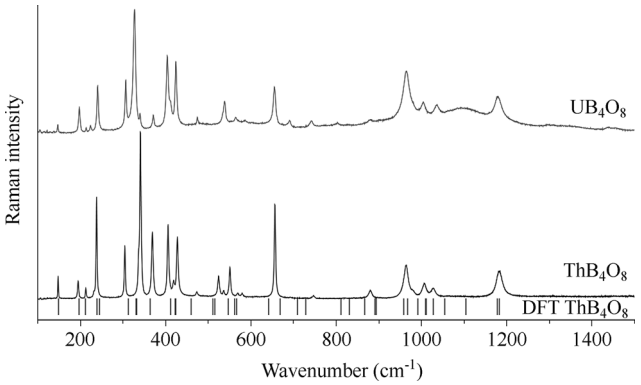

Figure 8. Raman spectra of single crystals of UB_4O_8 (top) and ThB_4O_8 (bottom) and theoretical bands of ThB_4O_8 (lines) within the range 100–1500 cm^{-1}.

could be detected within the range 3000–3600 cm^{-1}. Bands at about 900 cm^{-1} in borate compounds are usually assigned to the stretching modes of the $[BO_4]^{5-}$ groups. However, trigonal $[BO_3]^{3-}$ groups are expected at wavenumbers above 1150 cm^{-1}.[37–40] No bands are observed above 1200 cm^{-1}, as expected from the crystal structure due to the absence of trigonal $[BO_3]^{3-}$ groups. Bands at smaller wavenumbers than 500 cm^{-1} can be assigned to An–O (An = Th, U) bonds, to lower-wavenumber-shifted bending and stretching modes of tetrahedral $[BO_4]^{5-}$ groups, and to lattice vibrations. The large variation in B–O distances and in the linkage of the tetrahedral $[BO_4]^{5-}$ groups led to various experimentally observed modes.

FTIR-ATR measurements of the products (mixture of the actinide borate, unreacted actinide oxide, and a still-unknown phase) were performed to exclude water or hydrated borates. The spectra showed no bands within the region 3000–4000 cm^{-1}.

Quantum-mechanical calculations of the harmonic vibrational frequencies: To validate the quality of the basis sets and the functional, a geometry optimization of ThB_4O_8 was performed. Starting from the single-crystal structure, the geometry optimization yielded deviations in the lattice parameters and the atomic positions of less than 1%. The calculations of the harmonic vibrational frequencies were per-

formed on the optimized geometry. The calculated Raman bands fit quite well with the experimental spectrum of single crystals of ThB_4O_8. The low deviations were obtained from the approximations in the DFT method and the calculations on just one unit cell. Calculations of larger systems (super cells of ThB_4O_8) were not possible. Moreover, the calculation did not consider the temperature (297 K for the experiment) and the addition of two Gaussian peaks in the experimental spectrum led to a shift of the maxima. Table 7 lists

Table 7. Comparison and assignment of selected theoretical and experimental boron–oxygen bands in the Raman spectra of ThB_4O_8.[a]

Theoretical band [cm^{-1}]	Experimental band [cm^{-1}]	Assignment
1179, 1182	1183	b(B1-O3-B2), b(O1-B1-O2), b(O2-B2-O1), b(O2-B2-O3), s(B2–O4)
1056	1077	s(B2–O2)
1029	1028	s(B1–O2), b(O3-B2-O2), b(O4-B2-O2)
1010, 1013	1008	s(O3-B1-O2), s(B2–O4), b(O2-B2-O4), b(O3-B2-O4)
992	981	s(O2-B2-O4)
959, 969	964	s(O3-B1-O2), s(O4-B2-O3), s(B2–O3)
868, 892	880	s(B1–O1), b(O1-B2-O2)
643, 669	657	b(O2-B1-O3), b(O2-B2-O3), b(O4-B2-O3)

[a] s = Stretching mode, b = bending mode; pairs of bonded atoms with a large relative motion between them are given in parentheses.

the modes above 600 cm^{-1}. These bands can be assigned to boron–oxygen bending or stretching modes. However, in the assignment, the highly condensed boron–oxygen layers must be considered. An exclusive stretching or bending motion inside a tetrahedral $[BO_4]^{5-}$ group was not possible. Each stretching or bending motion induced motions of neighboring atoms. As expected, the calculation yielded no vibrational modes above 1200 cm^{-1}. The evaluation of the theoretical modes exclusively showed the impossibility of the assignment of one band to a particular stretching or bending mode inside the $[BO_4]^{5-}$ group. For example, the two modes at 1179 and 1182 cm^{-1} derive their origin from a various number of vibrational modes in the boron–oxygen layer.

Conclusion

Herein, we have described the high-pressure, high-temperature syntheses, single-crystal structural determinations, spectroscopic investigations, and theoretical calculations of the new actinide borates ThB_4O_8 and UB_4O_8. The crystal structures are constructed from layers of linked BO_4 tetrahedra. These layers contain threefold-coordinated oxygen atoms. The actinide cations are located between the boron–oxygen layers. In the future, we will attempt the synthesis of isotypic compounds with other cations in the oxidation state 4+ that have similar ionic radii, such as Ce^{4+}, by using the multianvil high-pressure technique. Furthermore, this research into actinide borates will be a good starting point for synthesizing the first actinide fluoride borate, in analogy to our work in the field of rare-earth fluoride borates.

Experimental Section

Caution: Working with UO_3 and ThO_2 requires appropriate precautions for the handling of radioactive and toxic substances.

Synthesis: The syntheses of AnB_4O_8 (*An* = Th, U) took place under high-pressure, high-temperature conditions. The synthesis of ThB_4O_8 was carried out at 5.5 GPa and 1100 °C, whilst the isotypic compound UB_4O_8 was synthesized at 10.5 GPa and 1100 °C. Depending on the actinide borate, stoichiometric mixtures of ThO_2 (synthesized by the decomposition of $Th(NO_3)_4{\cdot}4H_2O$ at 750 °C) or UO_3 (synthesized by the pyrolysis of $UO_2(NO_3)_2{\cdot}6H_2O$ at 300 °C) and B_2O_3 (Strem Chemicals, +99.9 %) in a 1:2 molar ratio were finely ground together, added into a platinum capsule, and placed in a boron-nitride crucible (Henze BNP GmbH, HeBoSint S100, Kempten, Germany). Then, the crucibles were placed into the center of an 18/11 assembly (for the thorium borate) or into the center of a 14/8 assembly (for the uranium borate). All of the synthetic steps were performed inside a glove box. The assemblies were compressed by using eight tungsten-carbide cubes (TSM-10 Ceratizit, Reutte, Austria). To apply the pressure, a 1000 ton multianvil press with a Walker-type module (both devices were purchased from Voggenreiter, Mainleus, Germany) was used. The assembly and its preparation are described in refs. [41–45]. For the synthesis of ThB_4O_8, the 18/11 assembly was compressed up to 5.5 GPa over 160 min, then heated at 1100 °C (in a cylindrical graphite furnace) over 10 min, kept at that temperature for 10 min, and cooled to 450 °C over 25 min at constant pressure. UB_4O_8 was synthesized by compressing the 14/8 assembly up to 10.5 GPa over 280 min, then heated at 1100 °C (in a cylindrical graphite furnace) over 10 min, kept at that temperature for 10 min, and cooled to 450 °C over 25 min at constant pressure. After natural cooling to RT by switching off the heating, decompression periods of 8 and 14 h were required. The recovered octahedral pressure medium (MgO, Ceramic Substrates & Components Ltd., Newport, Isle of Wight, UK) was broken apart and the samples were carefully separated from the surrounding graphite and boron nitride. Whilst ThB_4O_8 was obtained as colorless crystals, UB_4O_8 was obtained as green, air- and water-resistant crystals in a black matrix.

Crystal-structure analysis: The powder X-ray diffraction pattern of AnB_4O_8 (*An*=Th, U) were obtained in transmission geometry from flat samples of the reaction product on a STOE STADI P powder diffractometer with $Mo_{K\alpha1}$ radiation (Ge monochromator, $\lambda = 70.93$ pm). Figure 1 shows the experimental powder X-ray diffraction patterns of ThB_4O_8 and UB_4O_8, which matched well with the theoretical patterns that were simulated from the single-crystal data. The respective diffraction patterns showed reflections of ThB_4O_8 or UB_4O_8, unreacted ThO_2 or $UO_{2.12}$ (denoted with lines in Figure 1), and, in both cases, a still-unknown phase (denoted with circles in Figure 1). Small single crystals of ThB_4O_8 and UB_4O_8 were isolated by mechanical fragmentation. The single-crystal intensity data were collected at RT on a Nonius Kappa-CCD diffractometer with graphite-monochromated $Mo_{K\alpha}$ radiation ($\lambda = 71.073$ pm). A semiempirical absorption correction based on equivalent and redundant intensities (Scalepack[46]) was applied to the intensity data. All of the relevant details of the data collection and evaluation are listed in Table 1 for both compounds. The structure solution and parameter refinement

(full-matrix least-squares against F^2) were performed by using the SHELX-97 software suite.[47,48] According to the systematic extinctions, the monoclinic space group $C2/c$ was derived in both cases. All of the atoms were refined with anisotropic displacement parameters and the final difference Fourier syntheses did not reveal any significant peaks in both refinements. Tables 2–6 list the positional parameters, anisotropic displacement parameters, interatomic distances, and angles in these structures.

CSD-426310 (ThB_4O_8) and CSD-426311 (UB_4O_8) contain the supplementary crystallographic data for this paper. These data can be obtained from the Fachinformationszentrum Karlsruhe via http://www.fiz-informationsdienste.de/en/DB/icsd/depot_anforderung.html.

Vibrational spectra: Confocal Raman spectra of single crystals of AnB_4O_8 (An = Th, U) within the range 50–4000 cm^{-1} were recorded on a Horiba Jobin Yvon Labram-HR 800 Raman microspectrometer. The samples were excited by using the 532 nm emission line of a frequency-doubled 100 mW Nd:YAG laser and by using the 633 nm emission line of a 17 mW HeNe laser with an Olympus ×50 objective lens. The diameter of the laser spot on the surface was approximately 1 μm. The scattered light was dispersed by using an optical grating with 1800 lines mm^{-1} and collected by using a 1024×256 open-electrode CCD detector. The spectroscopic resolution, as determined by measuring the Rayleigh line, was less than 2 cm^{-1}. The spectra were recorded unpolarized. The accuracy of the Raman line shifts, as calibrated by regularly measuring the Rayleigh line, was on the order of 0.5 cm^{-1}. Background and Raman bands were fitted by using the built-in spectrometer software LabSpec to a second-order polynomial and convoluted Gaussian–Lorentzian functions, respectively.

The FTIR-ATR (Attenuated Total Reflection) spectra of powdered samples were measured on a Bruker Alpha-P spectrometer with a diamond ATR-crystal (2×2 mm) that was equipped with a DTGS detector within the spectroscopic range 400–4000 cm^{-1} (resolution: 4 cm^{-1}). 24 scans of the sample were acquired. A correction for atmospheric conditions was performed by using OPUS 7.0 software.

DFT calculations: In addition to the experimentally recorded IR and Raman spectra of ThB_4O_8, quantum-chemical computations of harmonic vibrational frequencies were performed by using the Crystal 09 program.[49–51] An important step in any quantum-mechanical calculation is the choice of an adequate basis set and a compromise must often be found between balancing computational effort and the accuracy of the results. To decrease the computational effort, a basis set with an effective core potential (ECP) for thorium was chosen. A suitable basis set for the actinide atom was identified based on geometry optimizations of ThB_4O_8. All-electron basis sets were employed for boron[52] and oxygen atoms.[53] Out of the results on the geometry optimization of ThB_4O_8, the well-tested ECP78MWB GUESS[54] basis set was chosen for the thorium atom. All of the calculations were performed by using the PBESOL functional[55] for the correlation and exchange functionals and the SCF convergence for the energy was set at $\times 10^{-12}$ E_h. The overall computation time for the calculations of the harmonic vibrational frequencies of ThB_4O_8 took 168 h on a cluster with 12 Intel Xeon CPU X5670 2.93 GHz processors.

Acknowledgements

We thank Dr. Peter Brunner (Universität Innsbruck) for his fruitful discussions. This research was funded by the Austrian Science Fund (FWF, P 23212-N19). F.K. thanks the DFG for a Heisenberg fellowship.

[1] H. Huppertz, *Chem. Commun.* **2011**, *47*, 131.
[2] H. Huppertz, B. von der Eltz, *J. Am. Chem. Soc.* **2002**, *124*, 9376.
[3] J. Knyrim, F. Roeßner, S. Jakob, D. Johrendt, I. Kinski, R. Glaum, H. Huppertz, *Angew. Chem.* **2007**, *119*, 9256; *Angew. Chem. Int. Ed.* **2007**, *46*, 9097.
[4] S. C. Neumair, S. Vanicek, R. Kaindl, D. Többens, C. Martineau, F. Taulelle, J. Senker, H. Huppertz, *Eur. J. Inorg. Chem.* **2011**, *27*, 4147.
[5] S. Wu, S. Wang, J. Diwu, W. Depmeier, T. Malcherek, E. V. Alekseev, T. E. Albrecht-Schmitt, *Chem. Commun.* **2012**, *48*, 3479.
[6] S. Wang, T. G. Parker, D. J. Grant, J. Diwu, E. V. Alekseev, W. Depmeier, L. Gagliardi, T. E. Albrecht-Schmitt, *Inorg. Chem.* **2012**, *51*, 11211.
[7] S. Wang, E. V. Alekseev, D. Juan, W. H. Casey, B. L. Phillips, W. Depmeier, T. E. Albrecht-Schmitt, *Angew. Chem.* **2010**, *122*, 1057.
[8] S. Wu, S. Wang, M. Polinski, O. Beerbaum, P. Kegler, T. Malcherek, A. Holzheid, W. Depmeier, D. Bosbach, T. E. Albrecht-Schmitt, E. V. Alekseev, *Inorg. Chem.* **2013**, *52*, 5110.
[9] M. J. Polinski, D. J. Grant, S. Wang, E. V. Alekseev, J. N. Cross, E. M. Villa, W. Depmeier, L. Gagliardi, T. E. Albrecht-Schmitt, *J. Am. Chem. Soc.* **2012**, *134*, 10682.
[10] S. Wang, E. V. Alekseev, J. T. Stritzinger, W. Depmeier, T. E. Albrecht-Schmitt, *Inorg. Chem.* **2010**, *49*, 2948.
[11] M. J. Polinski, S. Wang, E. V. Alekseev, W. Depmeier, G. Liu, R. G. Haire, T. E. Albrecht-Schmitt, *Angew. Chem. Int. Ed.* **2012**, *51*, 1869.
[12] A. Cousson, M. Gasperin, *Acta Cryst.* **1991**, *47*, 10.
[13] R. Naslain, J. Etourneau, J. S. Kasper, *J. Solid State Chem.* **1971**, *3*, 101.
[14] M. Gasperin, *Acta Cryst.* **1987**, *43*, 2031.
[15] C. Keller, K. H. Walter, *J. Inorg. Nucl. Chem.* **1965**, *27*, 1247.
[16] J. J. Berzelius, *Poggendorff's Ann. Phys* **1829**, *92*, 385.
[17] H. Huppertz, *Z. Naturforsch.* **2003**, *58b*, 278.
[18] H. Emme, H. Huppertz, *Z. Anorg. Allg. Chem.* **2002**, *628*, 2165.
[19] H. Emme, H. Huppertz, *Chem. Eur. J.* **2003**, *9*, 3623.
[20] H. Emme, H. Huppertz, *Acta Cryst.* **2005**, *C61*, i29.
[21] H. Huppertz, H. Emme, *J. Phys. Condens. Matter* **2004**, *16*, 1283.
[22] G. Heymann, T. Soltner, H. Huppertz, *Solid State Sci.* **2006**, *8*, 821.
[23] A. Haberer, G. Heymann, H. Huppertz, *Z. Naturforsch.* **2007**, *62b*, 759.
[24] The naming of the rings of the structural elements was coined by F. Liebau in *Structural Chemistry of Silicates*, Springer, Berlin, **1985**. It is derived from German numbers, e.g., the terms "dreier rings", "vierer rings", and "sechser rings" are derived from the words "drei", "vier", and "sechs", which translate to three, four, and six, respectively. However, the terms "dreier ring", "vierer ring", and "sechser ring" do not mean three-membered, four-membered, and six-membered rings, but rather rings with three, four, and six tetrahedral centers (B) and three, four and six electronegative atoms (O), respectively.
[25] E. Zobetz, *Z. Kristallogr.* **1990**, *191*, 45.
[26] F. C. Hawthorne, P. C. Burns, J. D. Grice in *Boron: Mineralogy, Petrology and Geochemistry* (Ed.: E. S. Grew), Mineralogical Society of America, Washington, **1996**.
[27] E. Zobetz, *Z. Kristallogr.* **1982**, *160*, 81.
[28] I. D. Brown, D. Altermatt, *Acta Cryst.* **1985**, *B41*, 244.
[29] N. E. Brese, M. O'Keeffe, *Acta Cryst.* **1991**, *B47*, 192.
[30] R. Hoppe, S. Voigt, H. Glaum, J. Kissel, H. P. Müller, K. J. Bernet, *J. Less-Common Met.* **1989**, *156*, 105.
[31] R. Hoppe, *Angew. Chem.* **1966**, *78*, 52; *Angew. Chem. Int. Ed. Engl.* **1966**, *5*, 95.
[32] R. Hoppe, *Angew. Chem.* **1970**, *82*, 7; *Angew. Chem. Int. Ed. Engl.* **1970**, *9*, 25.
[33] R. Hübenthal, *MAPLE*, Program for the Calculation of MAPLE Values, *Version 4*, University of Gießen, Gießen, **1993**.
[34] M. Idiri, T. Le Bihan, S. Heathman, J. Rebizant, *J. Phys.: Condens. Matter.* **2003**, *15*, 2297.
[35] R. E. Rundle, N. C. Baenzinger, A. S. Wilson, R. A. McDonald, *J. Am. Chem. Soc.* **2008**, *130*, 3296.
[36] C. T. Prewitt, R. D. Shannon, *Acta Cryst.* **1968**, *B24*, 869.
[37] H. Huppertz, *J. Solid State Chem.* **2004**, *177*, 3700.
[38] L. Jun, X. Shuping, G. Shiyang, *Spectrochim. Acta Part A* **1995**, *51*, 519.
[39] G. Chadeyron, M. El-Ghozzi, R. Mahiou, A. Arbus, J. C. Cousseins, *J. Solid State Chem.* **1997**, *128*, 261.
[40] J. C. Zhang, Y. H. Wang, X. Guo, *J. Lumin.* **2007**, *122–123*, 980.

[41] N. Kawai, S. Endo, *Rev. Sci. Instrum.* **1970**, *41*, 1178.
[42] D. Walker, M. A. Carpenter, C. M. Hitch, *Am. Mineral.* **1990**, *75*, 1020.
[43] D. Walker, *Am. Mineral.* **1991**, *76*, 1092.
[44] D. C. Rubie, *Phase Trans.* **1999**, *68*, 431.
[45] H. Huppertz, *Z. Kristallogr.* **2004**, *219*, 330.
[46] Z. Otwinowski, W. Minor, *Methods Enzymol.* **1997**, *276*, 307.
[47] G. M. Sheldrick, SHELXS-97 and SHELXL-97, Program Suite for the Solution and Refinement of Crystal Structures, University of Göttingen, Göttingen, **1997**.
[48] G. M. Sheldrick, *Acta Cryst.* **2008**, *A46*, 112.
[49] R. Dovesi, V. R. Saunders, C. Roetti, R. Orlando, C. M. Zicovich-Wilson, E. Pascale, B. Civalleri, K. Doll, N. M. I. J. Bush, Ph. D'Arco, M. Llunell, CRYSTAL09-User's Manual, University of Torino, Torino, **2009**.
[50] R. Dovesi, R. Orlando, B. Civalleri, R. Roetti, V. R. Saunders, C. M. Zicovich-Wilson, *Z. Kristallogr.* **2005**, *220*, 571.
[51] F. Pascale, C. M. Zicovich-Wilson, F. Lopez, B. Civalleri, R. Orlando, R. Dovesi, *J. Comput. Chem.* **2004**, *25*, 888.
[52] R. Orlando, R. Dovesi, C. Roetti, *J. Phys. Condens. Matter* **1990**, *2*, 7769.
[53] L. Valenzano, F. J. Torres, K. Doll, F. Pascale, C. M. Zicovich-Wilson, R. Dovesi, *Z. Phys. Chem. (München Ger.)* **2006**, *220*, 893.
[54] A. Moritz, X. Cao, M. Dolg, *Theor. Chem. Acc.* **2007**, *118*, 845.
[55] J. P. Perdew, A. Ruzsinszky, G. I. Csonka, O. A. Vydrov, G. E. Scuseria, L. A. Constantin, X. Zhou, K. Burke, *Phys. Rev. Lett.* **2008**, *100*, 136406.

Received: June 21, 2013
Published online: October 10, 2013

